Bulletin of the Seismological Society of America, Vol. 93, No. 4, pp. 1773–1791, August 2003

Evaluation of Short-Period, Near-Regional M_s Scales for the Nevada Test Site

by Jessie L. Bonner, David G. Harkrider, Eugene T. Herrin, Robert H. Shumway, Sara A. Russell, and Ileana M. Tibuleac

Abstract Surface wave magnitude (M_s) estimation for small events recorded at near-regional distances will often require a magnitude scale designed for Rayleigh waves with periods less than 10 sec. We have examined the performance of applying two previously published M_s scales on 7-sec Rayleigh waves recorded at distances less than 500 km. First, we modified the Marshall and Basham (1972) M_s scale, originally defined for periods greater than 10 sec, to estimate surface wave magnitudes for short-period Rayleigh waves from earthquakes and explosions on or near the Nevada Test Site. We refer to this modification as $\overset{M+B}{M_s}(7)$, and we have used short-period, high-quality dispersion curves to determine empirical path corrections for the 7-sec Rayleigh waves. We have also examined the performance of the Rezapour and Pearce (1998) formula, developed using theoretical distance corrections and surface wave observations with periods greater than 10 sec, for 7-sec Rayleigh waves ($\overset{R+P}{M_s}(7)$) as recorded from the same dataset. The results demonstrate that both formulas can be used to estimate M_s for nuclear explosions and earthquakes over a wider magnitude distribution than is possible using conventional techniques developed for 20-sec Rayleigh waves. These $M_s(7)$ values scale consistently with other M_s studies at regional and teleseismic distances with the variance described by a constant offset; however, the offset for the $\overset{M+B}{M_s}(7)$ estimates is over one magnitude unit nearer the teleseismic values than the $\overset{R+P}{M_s}(7)$ estimates. Using our technique, it is possible to employ a near-regional single-station or sparse network to estimate surface wave magnitudes, thus allowing quantification of the size of both small earthquakes and explosions. Finally, we used a jackknife technique to determine the false-alarm rates for the $\overset{M+B}{M_s}(7)$-m_b discriminant for this region and found that the probability of misclassifying an earthquake as an explosion is 10%, while the probability of classifying an explosion as an earthquake was determined to be 1.2%. The misclassification probabilities are slightly higher for the $\overset{R+P}{M_s}(7)$ estimates. Our future research will be aimed at examining the transportability of these methods.

Introduction

One of the most robust methods for discriminating between explosions and earthquakes is the relative difference between the body wave (m_b) and surface wave (M_s) magnitude for a seismic event. For a given m_b, earthquakes often generate substantially more surface wave energy than explosions and thus are characterized by a larger surface wave magnitude. M_s scales include those defined for Rayleigh waves with periods near 20 sec recorded at teleseismic distances (Gutenberg, 1945; von Seggern, 1977; Yacoub, 1983) as well as scales developed for variable periods at both regional and teleseismic distances (e.g., the Prague formula of Vanek *et al.*, 1962; Basham, 1971; Evernden, 1971; Marshall and Basham, 1972; Rezapour and Pearce, 1998). The predominance of M_s measurements determined for explosion sources using these formulae are for events with m_b greater than 4.5; thus, there is uncertainty in the M_s-m_b discriminant performance for explosions with smaller m_b, corresponding to yields of less than approximately 20 kt.

None of the aforementioned studies have attempted to determine if magnitudes obtained from surface waves re-

corded at near-regional distances and periods less than 10 sec can be used to accurately characterize the size of a seismic source. The answer to this question is essential in determining our ability to discriminate lower-yield events in the $3.5 < m_b < 4.5$ range. Levshin and Ritzwoller (2001) suggested this problem is difficult to answer because structural variations that alter short-period surface wave amplitudes by as much as 50% have scales that cannot be resolved with current 3D models, thus rendering path corrections difficult to determine. Also, short-period surface waves are more sensitive to high-frequency asymmetries in the shot cavity (Zhao and Harkrider, 1992) and spall (Taylor and Randall, 1989; Day and McLaughlin, 1991). The fact remains, however, that at regional distances, surface wave trains are not well dispersed and are often characterized by a pulselike shape with dominant periods ranging from 5 to 12 sec. Thus, it is difficult, and for small events often impossible, to determine an M_s as it was originally defined for 20-sec Rayleigh waves. Either a path-corrected, spectral magnitude (e.g., Stevens and McLaughlin, 2001; Stevens and Murphy, 2001) or an M_s scale that can incorporate these shorter periods is required to examine the performance of the M_s-m_b discriminant for small events recorded at regional distances.

The purpose of this article is to present the results of applying two established and popular M_s formulas, both developed using surface waves with periods between 10 and 20 sec, on 7-sec, near-regional, Rayleigh-wave data. First, we modified the Marshall and Basham (1972) M_s scale, originally defined for periods greater than 10 sec, to estimate surface wave magnitudes for 7-sec Rayleigh waves. We refer to this modification as $\overset{M+B}{M}_s(7)$. We based our decision to use 7-sec Rayleigh waves on observations that this period (1) represents an average of the dominant energy for surface waves recorded at near-regional distances near the Nevada Test Site (NTS) and (2) is far enough from Airy-phase phenomena so that path corrections can be estimated. We have applied our $\overset{M+B}{M}_s(7)$ to 158 NTS explosions and 40 earthquakes recorded at near-regional distances ($<$1000 km). We have also applied the Rezapour and Pearce (1998) formula to this dataset and refer to this estimate as $\overset{R+P}{M}_s(7)$. Finally, we used estimates from both of these scales to examine the $M_s(7)$-m_b discriminants for the western United States (WUS).

Data

The data are vertical-component, digital broadband seismograms from NTS explosions and WUS earthquakes recorded on the four stations of the Lawrence Livermore Regional Seismic network (LNN). The LNN consists of seismic stations at Landers, California (LAC), Mina, Nevada (MNV), Elko, Nevada (ELK), and Kanab, Utah (KNB) and has been in operation since the 1960s (Fig. 1). The data recorded at these stations originally consisted of analog seismograms,

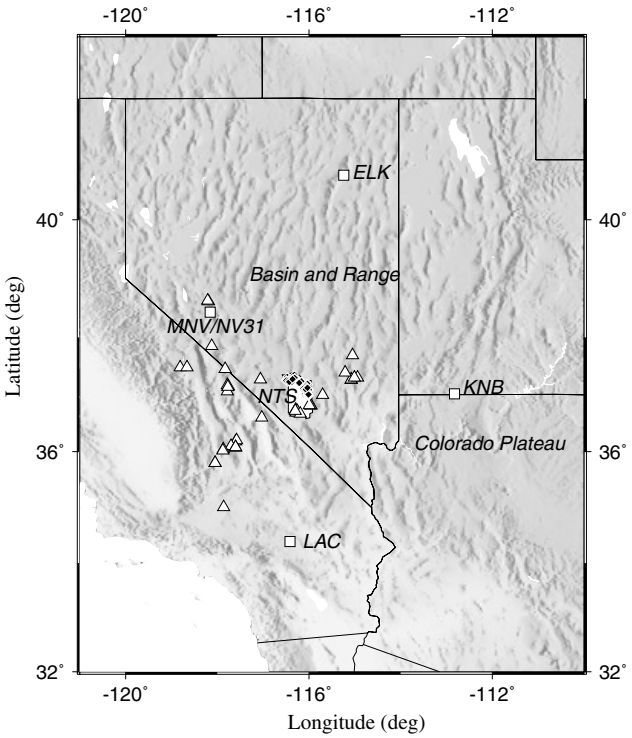

Figure 1. The locations of the four LNN stations (white squares), as well as earthquakes (white triangles) and explosions (black diamonds on the NTS) used in this study.

which were subsequently digitized by Lawrence Livermore National Laboratory. The analog instruments were replaced in July 1979 by digital systems, which have been in almost continuous operation since, resulting in an extensive record of the testing conducted at the NTS. In December 1998, an International Monitoring System station, NV31 (Fig. 1), was colocated with MNV, and we have included data from this station for this research. Although there are additional stations in the region for which data are available, we chose not to use them since one of our research goals was to examine how well a regional surface wave magnitude scale can perform using sparse data. This is an important aspect of the research since small-yield events will be recorded on relatively few regional stations.

We have estimated surface wave magnitudes for NTS explosions that occurred between December 1968 and September 1992. The primary research focus was on the 198 NTS explosions (Yang *et al.*, 2000) that were detonated after August 1979, for which digital data are available from the LNN stations. Sixty-one of these events have no LNN data available, are plagued by untimely data dropouts and glitches, or are too small for measurable surface wave energy. We also analyzed 21 events prior to July 1979 that were digitized from analog records in order to compare these results with previous M_s studies for NTS events completed by Yacoub (1983), Marshall *et al.* (1979), and Stevens and Murphy (2001). Thus, this article presents the results of our

analyses of 158 NTS explosions, including 51 events from Pahute Mesa, 13 from Rainier Mesa, and 94 explosions from the Yucca Flats. We have also tabulated the location of the events relative to the water table and the lithology in which the event was detonated.

We also estimated the M_s and m_b magnitudes for 40 earthquakes, whose locations are shown in Figure 1. The earthquake data consisted of LNN seismograms for events tabulated in table A.1 of Patton (2001) that were within 2° of the NTS. This allowed us to maintain similar azimuthal coverage and propagation paths for the NTS explosions in our dataset. The Patton (2001) earthquake database has no events beyond 1994; thus we also downloaded data recorded at station NV31 for events between January 1999 and June 2002. This earthquake dataset, while not as extensive as our explosion database, has $m_b(Pn)$ (Patton, 2001) values ranging from 2.98 to 5.84 and depths ranging from 0 to 17 km.

Methodology

Examples of near-regional, fundamental-mode surface waves recorded at MNV from five different source regions of the WUS are shown in Figure 2. These surface waves have been extracted from the MNV vertical broadband components through phase-matched filtering (Herrin and Goforth, 1977). All five of these events are in the $3.7 < m_b < 4.1$ range, and none of the events have Rayleigh-wave periods greater than 12 sec. The largest amplitude for the events occurs at periods between 6 sec (Mammoth Lake earthquake) and 9 sec (Little Skull Mountain earthquake). Denny *et al.* (1987) showed some success at obtaining the regional M_s for similar earthquakes and explosions in this region and expressed the need for accurate path corrections to maximize the M_s-m_b discriminant performance. This article differs from their methodology in three ways: (1) we obtain the path corrections directly from observed dispersion curves instead of from regional velocity models; (2) we use a processing technique developed to positively identify small-amplitude, fundamental-mode Rayleigh-wave motion; and (3) we calculate the M_s for Rayleigh waves of 7-sec period as opposed to variable periods. We are not aware of other M_s scales that have been developed and tested for 7-sec Rayleigh waves at near-regional distances and calibrated using conventional M_s estimates.

m_b Estimation

For our examination of the M_s-m_b discriminant performance for small events in the WUS, we required both regional m_b and M_s magnitude scales. Fortunately, an m_b scale has already been developed and tested for the WUS. The Denny *et al.* (1987, 1989) body wave magnitude formula (referred to as the DTV m_b) was specifically developed for

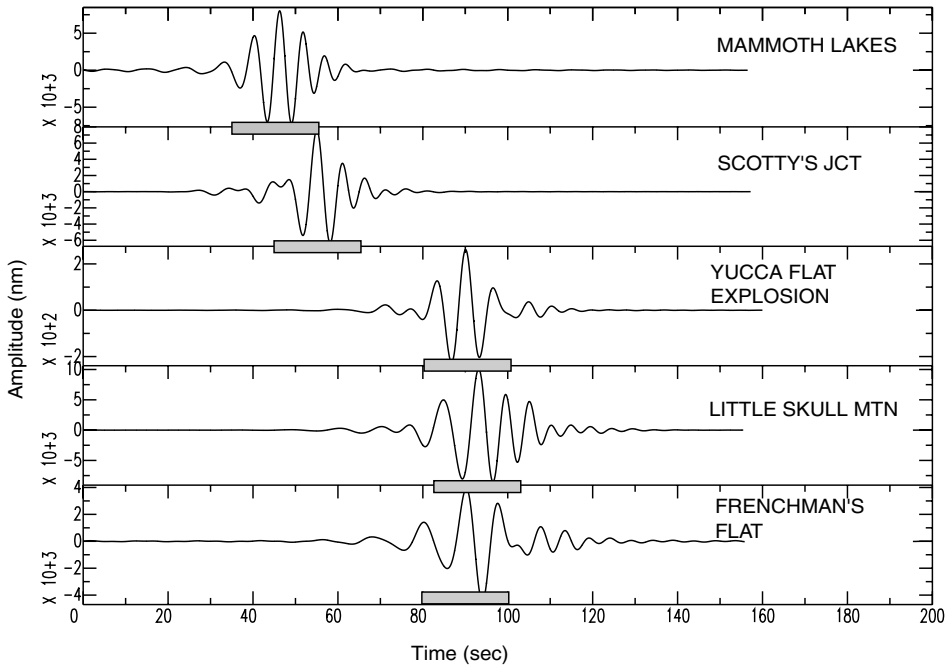

Figure 2. Examples of near-regional, fundamental-mode Rayleigh waves extracted from events near Mammoth Lakes, California, Scotty's Junction, Nevada, Yucca Flats on the Nevada Test Site (NTS), Little Skull Mountain (NTS), and Frenchman's Flat (NTS). The events are earthquakes with the exception of the Yucca Flats explosion. None of these events ($3.7 < m_b < 4.1$) exhibit surface wave periods greater than 12 sec; the maximum amplitudes occur at periods between 5 and 9 sec. The bar plotted below each seismogram corresponds to a length of 20 sec.

the WUS using an extensive database of earthquakes and nuclear explosions at or near the NTS. They defined their m_b scale for *Pn* arrivals as

$$m_b(Pn) = \log(A) + 2.4 \log(d) - 3.95 + C, \quad (1)$$

where A is the peak-to-peak amplitude in nanometers, d is the distance in kilometers, and C is a station constant empirically determined to be -0.02 for MNV, -0.13 for ELK, -0.19 for KNB, and $+0.33$ for LAC (Denny *et al.*, 1989). Subsequently, Tibuleac *et al.* (2002) showed the constant at NV31 (-0.018) was approximately equal to the MNV constant. The amplitude measurements were made on simulated short-period Worldwide Standard Seismographic Network response seismograms. This magnitude scale was correlated to the yield of the NTS explosions and therefore does not have a network bias problem for small-magnitude events. All m_b's presented in this study are $m_b(Pn)$'s estimated using equation (1). For most of the NTS explosions, we used the $m_b(Pn)$ determined by Vergino and Mensing (1989), and we used the $m_b(Pn)$ determined by Patton (2001) for most of the WUS earthquakes. For events in which no $m_b(Pn)$ was published, we used equation (1) to calculate an average network $m_b(Pn)$ using the available LNN stations.

Surface Wave Processing

Near-regional surface waves in the WUS have their largest amplitudes occurring at periods between 5 and 9 sec (Fig. 2), and these amplitudes can often be 6–10 dB larger than the amplitudes measured at 20-sec period. We have shown (Tibuleac *et al.*, 2002) that for NTS events recorded at MNV, the energy in 20-sec Rayleigh waves subsides below background noise levels at approximately $m_b = 4.3 \pm 0.2$. Therefore, M_s scales that consider surface waves between 5 and 9 sec will be applicable to lower m_b values. It is important to note that caution must be used to ensure that the measured signals are, in fact, Rayleigh waves and not microseisms, higher-mode energy, or Love wave contamination.

We employ a surface wave processing routine that is designed to help positively identify small-amplitude, fundamental-mode, Rayleigh-wave motion. The method is applied to all explosions with $m_b < 4.0$ (and for earthquakes with $m_b < 3.5$), since the signal-to-noise ratio (SNR) for larger events is great enough that amplitude measurements can be made by bandpass filtering the velocity records and measuring the amplitudes in a group velocity window indicative of 7-sec Rayleigh waves in the WUS. For explosions with $m_b < 4.0$, we first use the multiple filter analysis technique (Dziewonski *et al.*, 1969) to generate a group velocity dispersion curve for each event-to-station path. We then overlay the theoretical fundamental-mode and first-higher-mode dispersion curves predicted for the path from the Stevens *et al.* (2001) global shear-wave model. We require at least 70% overlap (similar to Stevens and McLaughlin, 2001) in the observed dispersion, plus error in the 5- to 10-sec period band with the predicted fundamental-mode dispersion from the Stevens *et al.* (2001) model. If the event passes the dispersion test, we then determine if the signal has retrograde elliptical particle motion and a backazimuth that is within $\pm 30^\circ$ of the true backazimuth. We have followed the methods of Chael (1997) and Selby (2001) to determine the backazimuth that corresponds to the largest positive value, indicative of retrograde elliptical motion, in a covariance matrix formed by the Hilbert-transformed vertical component and the two horizontal components. If a given event passes the dispersion, backazimuth, and particle motion tests, we have positively identified fundamental-mode Rayleigh waves for the event of interest. It is critical that the event pass all three tests, since microseisms may occur in the correct group velocity window and possess retrograde elliptical motion with the correct backazimuth. However, our experience with these rare situations has shown that we will not observe the 70% overlap between the observed and predicted dispersion curve in the entire 5- to 10-sec band.

Once identified as fundamental-mode Rayleigh waves, we employ a phase match filter (PMF) technique (Herrin and Goforth, 1977) to extract the Rayleigh waves from the complex wave train. We use the observed group velocity dispersion curve for the event and an iterative approach (Herrmann, 2002) to find and apply a filter that has approximately the same phase as the Rayleigh-wave signal of interest. This technique improves the SNR for the extracted surface waves. We then perform a bandpass filter around a center period of 7 sec on the PMF-extracted signal. From this filtered data, the maximum zero-to-peak amplitude is measured, and this amplitude is then used to estimate $M_s(7)$.

Surface Wave Magnitude Estimation

$M_s(7)$ *from Marshall and Basham* (*1972*). Marshall and Basham (1972) reformulated the Prague formula (Vanek *et al.*, 1962) as

$$M_s = \log(A) + B'(\Delta) + P(T), \quad (2)$$

where A is the Rayleigh-wave amplitude (zero-to-peak in nanometers), $B'(\Delta)$ is an attenuation correction as a function of distance (Δ) in degrees, and $P(T)$ is a path correction as a function of period T. There is an additional term of $0.008h$ (Bath, 1952), where h is the depth of the event, that can be included in equation (2). Because depth is often difficult to determine for near-regional events, we did not apply a depth correction to the explosion and earthquake data in order to examine the discriminant performance assuming a surface focus. The distance corrections $B'(\Delta)$ (Table 1) used for this study are proportional to $0.8\log(\Delta)$, as Basham (1971) showed this relation to be valid for earthquakes and explosions with an 8- to 14-sec period at regional distances.

The path corrections listed in table 2 of Marshall and Basham (1972) are not applicable to periods less than 10 sec; however, our Figure 2 shows that path corrections are

Table 1
$B'(\Delta)$ Corrections for Near-Regional Distances

Distance (degrees)	$B'(\Delta)$
0.5	0.09
1.0	0.17
1.5	0.26
2.0	0.36
2.5	0.46
3.0	0.55
3.5	0.63
4.0	0.68
4.5	0.73
5.0	0.77

Table 2
P(T) Corrections

Station	$P(T)$
MNV/NV31	−0.79
ELK	−0.79
KNB	−0.56
LAC	−0.73

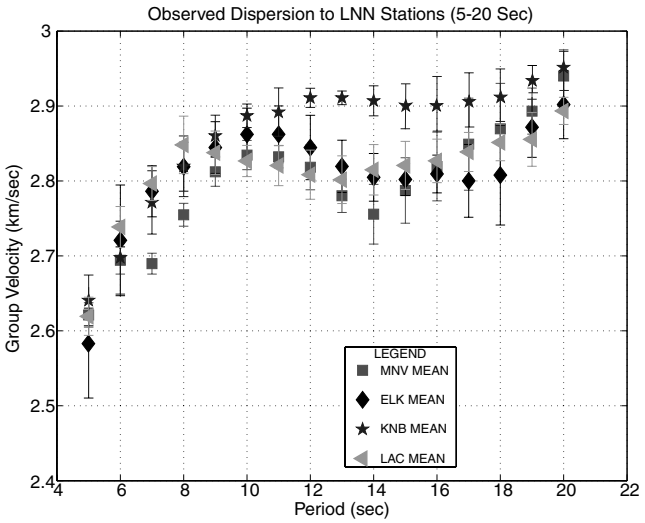

Figure 3. Average Rayleigh-wave group velocity dispersion curves obtained from the multiple filter analyses and phase-match filtering of eight NTS explosions with paths to MNV, ELK, KNB, and LAC. The dispersion curves were used to determine path corrections [$P(T)$]. The vertical lines through the dispersion data points represent one standard deviation.

needed for periods as low as 5 sec. The path correction $P(T)$ is estimated from the amplitude of a group velocity (U) dispersion curve predicted by the method of stationary phase (Ewing *et al.*, 1957) with the expression $U/T^{3/2}\sqrt{dU/dT}$. The $P(T)$ corrections are normalized to a 20-sec period in order to compare the short-period results with conventional M_s measurements. To generate the $P(T)$ corrections, we used multiple filter analyses to generate group velocity dispersion curves for paths from NTS to MNV, ELK, KNB, and LAC. We averaged the dispersion curves for eight NTS explosions with large Rayleigh-wave SNR ($m_b > 5.2$) between 5 and 20 sec, and the results are shown in Figure 3. We based our decision to make our surface wave measurements at a period of 7 sec on two observations. First, as shown in Figure 2, a period of 7 sec represents an average of the dominant periods for surface waves recorded at near-regional distances in the WUS. Additionally, Figure 3 shows there is an inverse Airy phase (or a group velocity maximum) observable on the dispersion curves near approximately 9-sec period, and it is best to retreat from the complications associated with this phenomenon when making amplitude measurements. As determined from the expression $U/T^{3/2}\sqrt{dU/dT}$, the $P(T)$ corrections will become infinite at each Airy phase. We determined the $P(7)$ corrections for each path, and the results are listed in Table 2. The $P(7)$ corrections for paths to MNV, ELK, and LAC are essentially the same since these paths are all located within the southern Basin and Range tectonic province (Fig. 1). The different dispersion curve for the path from NTS to KNB is caused by the thickening of the crust near the station associated with the transition from the Basin and Range to the Colorado Plateau (Keller *et al.*, 1976). We refer to our surface wave estimates for 7-sec Rayleigh waves using equation (2) and empirically calibrated path corrections as M_s^{M+B} (7).

$M_s(7)$ *from Rezapour and Pearce (1998).* Using the entire dataset from the International Seismic Center, Rezapour and Pearce (1998) developed a distance-independent M_s defined as

$$M_s = \log\frac{A}{T} + \frac{1}{3}\log(\Delta) + \frac{1}{2}\log(\sin(\Delta)) + 0.0046\Delta + 2.370, \quad (3)$$

where A is the zero-to-peak amplitude in nanometers, T is the period in seconds, and Δ is the distance in degrees. Unlike the Marshall and Basham (1972) formula that used empirical distance and path corrections (equation 2), the Rezapour and Pearce (1998) equation was developed using theoretical aspects of dispersion and geometrical spreading. The formula was adopted by the prototype International Data Center in 1998 for calculating surface wave magnitudes at distances between 20° and 100°; however, it is now used by the International Data Center to determine an M_s for all surface waves recorded at distances less than 100° (Stevens and McLaughlin, 2001). We note that the original Rezapour and Pearce (1998) paper presents no application of their formula at periods less than 10 sec and at distances less than 20°. For this study, we applied equation (3) to short-period, near-regional data to determine $M_s^{R+P}(7)$ estimates for the same

dataset as used for the modified Marshall and Basham (1972) formula.

Results

NTS Explosions

We measured the amplitude for 7-sec-period Rayleigh waves for 158 NTS events recorded at MNV, ELK, KNB, and LAC and estimated both $\overset{M+B}{M_s}(7)$ and $\overset{R+P}{M_s}(7)$ for each event. The results are compiled in Table 3 and are shown in Figures 4–7. Figure 4 examines the variability in both $M_s(7)$ estimates by comparing the MNV values to the $M_s(7)$ estimated at ELK (top), KNB (middle), and LAC (bottom). When we consider the effects that tectonic release can have on explosion magnitudes as well as the fact that small-scale structural variations have a magnified effect on shorter-period surface waves, we believe that the scatter in the data is tolerable. In all six cases, the correlation coefficient is at least 0.98. For all comparisons, we note that the slopes for the best least-squares fit to the data are slightly smaller than unity (0.90–0.95), resulting in positive y intercepts. The MNV $M_s(7)$ estimates are on average 0.15 magnitude units less than the LAC values. It is very hard to pinpoint the source of this bias. However, two possible explanations include inadequate path corrections, $P(T)$, or differences between the attenuation model used in equation (2) (Basham, 1971 for 8- to 14-sec surface waves) and equation (3) (Rezapour and Pearce, 1998) and the actual attenuation of 7-sec surface waves in the WUS. We note that for events with an $\overset{M+B}{M_s}(7) < 3.5$, the MNV estimates are on average smaller than the KNB estimates, while at greater magnitudes the KNB estimates are smaller. The reason for this difference is thought to be a spectral hole that occurs on the KNB data between 6- and 7-sec period that is more prevalent for the larger-magnitude events. Even with the presence of the spectral hole near 7 sec, we note that the maximum difference between the KNB and MNV estimates above $\overset{M+B}{M_s}(7) = 3.5$ is -0.4 m.u. with the average difference being less than -0.1 m.u. The results of these comparisons show that single-station (e.g., MNV) $\overset{M+B}{M_s}(7)$ and $\overset{R+P}{M_s}(7)$ estimates for NTS explosions are reliable (one standard deviation $< \pm 0.2$ m.u.) in the WUS when only sparse data are available.

We present a comparison of the network-averaged $\overset{M+B}{M_s}(7)$ and $\overset{R+P}{M_s}(7)$ for all measured NTS events versus the DTV network $m_b(Pn)$ in Figure 5. Pahute Mesa, Rainier Mesa, and Yucca Flats events were analyzed and are presented as circles, stars, and triangles, respectively. We also denote the location of the water table, relative to each event, as either a solid symbol (events that were detonated above the water table) or an open symbol (events detonated below the water table). We regressed the $\overset{M+B}{M_s}(7)$ and $\overset{R+P}{M_s}(7)$ versus the DTV $m_b(Pn)$, and the resulting equations and standard deviations for each NTS test area are shown.

The purpose of this article is not to examine scaling laws or coupling factors for the areas of the NTS; the reader is referred to Woods and Harkrider (1995) and Patton (1991) for further details concerning those topics. However, our results generally agree with Woods and Harkrider (1995), who suggested that there are different scaling relationships between Pahute Mesa and Yucca Flats events. The primary goals of our article are to present the applicability of the $M_s(7)$ scale and to highlight the fact that using the short-period data allows us to estimate surface wave magnitudes for 45 explosions with $m_b < 4.5$, as compared to 1 in the original Marshall and Basham (1972) paper, 2 in the Rezapour and Pearce (1998) paper, and less than 10 in Stevens and McLaughlin (2001). In addition, we have determined $M_s(7)$ measurements for nine events with $3.7 < m_b < 4.0$.

For the purpose of regional application of an $M_s(7)$ magnitude scale, it is unlikely that a network similar to LNN will be available for monitoring most nuclear test sites. Thus, we examined the relationship between single-station MNV $\overset{M+B}{M_s}(7)$ and $\overset{R+P}{M_s}(7)$ estimates and DTV $m_b(Pn)$ and present the results in Figure 6. For this analysis, we note that the regression results for the Yucca Flats events do not change significantly for the single-station $\overset{M+B}{M_s}(7)$ and $\overset{R+P}{M_s}(7)$ while there are differences for the results for Pahute Mesa and Rainier Mesa. In general, the "clouds" formed by the single-station $\overset{M+B}{M_s}(7)$ and $\overset{R+P}{M_s}(7)$ measurements do not change significantly from the results using network averages.

Comparison of the Near-Regional $M_s(7)$ and Teleseismic M_s

Of course, estimating near-regional $M_s(7)$ values for NTS events that can be calibrated to conventional M_s scales is of primary importance to our research as well. We compared our $\overset{M+B}{M_s}(7)$ and $\overset{R+P}{M_s}(7)$ estimates taken directly from the near-regional surface waves with the M_s measurements obtained from a modeling technique derived by Woods and Harkrider (1995). Their indirect method of estimating M_s consisted of modeling the surface waves recorded at regional distances and then propagating the regional synthetics to distances of 40°. At 40°, the synthetics showed significant 20-sec surface wave energy, and the authors used a modified von Seggern (1977) formula to measure M_s from the synthetics. Figure 7 shows the comparison of our $\overset{M+B}{M_s}(7)$ and $\overset{R+P}{M_s}(7)$ with $\pm 1\sigma$ plotted as the horizontal lines and the Woods and Harkrider (1995) indirect method with $\pm 1\sigma$ plotted as vertical lines. We performed a fixed-slope (slope $= 1$) linear regression to compare the $M_s(7)$ values with the Woods and Harkrider (1995) values and found a strong correlation. The offset shows that the $\overset{M+B}{M_s}(7)$ and $\overset{R+P}{M_s}(7)$ estimates are 0.20 m.u. lower and 0.95 m.u. higher, respectively,

Table 3
NTS Explosion Information

			M+B		R+P					
Date	Name	m_b	M_s	std	M_s	std	#	A	W	L
1968354	Benham	6.49	5.66	0.12	6.87	0.17	3	P	B	T
1969302	Calabash	5.5	4.44	0.09	5.72	0.04	2	Y	B	T
1970085	Handley	6.57	5.61	0.10	6.85	0.14	4	P	B	T
1970146	Flask	5.47	4.17	0.15	5.41	0.11	4	Y	A	T
1970351	Carpetbag	5.79	4.68	0.11	5.92	0.14	4	Y	B	T
1972265	Osocurro	5.6	4.47	0.06	5.68	0.16	3	Y	B	T
1972270	Delphinium	4.54	2.64	0.14	3.85	0.14	3	Y	A	A
1973116	Starwort	5.49	4.03	0.10	5.26	0.05	4	Y	B	T
1973157	Alemendro	6.23	5.07	0.20	6.35	0.23	3	P	B	R
1974191	Escabosa	5.54	4.49	0.01	5.69	0.15	2	Y	B	T
1975059	Topgallant	5.7	4.48	0.13	5.72	0.04	4	Y	B	T
1975154	Stilton	6.03	4.62	0.10	5.85	0.18	4	P	B	R
1975154	Mizzen	5.66	4.45	0.10	5.69	0.08	4	Y	B	T
1975170	Mast	6.24	5.03	0.15	6.26	0.19	4	P	B	R
1975324	Inlet	6.01	4.90	0.16	6.14	0.22	4	P	B	R
1975354	Chiberta	5.76	4.60	0.15	5.83	0.09	4	Y	B	T
1976035	Keelson	5.61	4.31	0.18	5.55	0.16	4	Y	B	T
1976035	Esrom	5.69	4.53	0.10	5.76	0.07	3	Y	B	T
1976045	Cheshire	6.13	5.03	0.12	6.26	0.17	4	P	B	R
1976069	Estuary	6.09	5.13	0.19	6.36	0.25	4	P	B	R
1976077	Strait	5.87	4.87	0.13	6.08	0.08	3	Y	B	T
1979215	Burzet	4.78	2.89	0.06	4.10	0.17	3	Y	A	A
1979220	Offshore	4.85	3.18	0.10	4.39	0.20	3	Y	A	T
1979241	Nessel	4.93	3.14	0.17	4.37	0.23	4	Y	A	A
1979249	Hearts	5.83	4.43	0.07	5.67	0.15	4	Y	B	T
1979269	Sheepshead	5.73	4.25	0.10	5.48	0.18	4	P	A	T
1980059	Tarko	4.43	2.69	0.17	3.91	0.11	3	Y	A	A
1980094	Liptauer	4.9	2.95	0.22	4.19	0.28	4	Y	A	A
1980107	Pyramid	5.45	4.05	0.24	5.29	0.30	4	Y	B	T
1980117	Colwick	5.66	4.30	0.14	5.53	0.22	4	P	B	R
1980123	Canfield	4.38	2.58	0.10	3.81	0.05	3	Y	A	T
1980164	Kash	5.61	4.41	0.11	5.62	0.20	3	P	B	R
1980176	Huron King	4.2	2.28	0.12	3.50	0.19	3	Y	A	A
1980207	Tafi	5.8	4.38	0.09	5.62	0.18	4	P	B	T
1980213	Verdello	4.12	2.50	0.10	3.77	0.13	2	Y	A	A
1980269	Bonarda	4.5	2.44	0.09	3.68	0.09	4	Y	A	T
1980298	Dutchess	4.43	2.82	0.13	4.06	0.11	4	Y	A	T
1980305	Miners Iron	4.65	3.02	0.16	4.25	0.21	4	R	A	T
1980319	Dauphin	4.39	2.72	0.05	3.96	0.14	4	Y	A	T
1980352	Serpa	5.26	3.77	0.11	5.01	0.17	4	P	A	T
1981015	Baseball	5.56	4.15	0.11	5.39	0.18	4	Y	B	T
1981149	Aligote	4.19	2.52	0.20	3.75	0.10	3	Y	A	T
1981157	Harzer	5.62	4.15	0.14	5.39	0.19	4	P	A	T
1981191	Niza	4.18	2.43	0.12	3.66	0.04	4	Y	A	T
1981239	Islay	3.96	2.08	0.08	3.39	0.06	2	Y	A	T
1981247	Trebbiano	3.98	1.87	0.16	3.10	0.18	4	Y	A	T
1981274	Paliza	5.12	3.69	0.37	4.93	0.40	4	Y	A	T
1981315	Tilci	4.9	3.16	0.06	4.40	0.16	4	Y	A	A
1981316	Rousanne	5.38	3.92	0.12	5.16	0.17	4	Y	B	T
1981337	Akavi	4.7	2.97	0.18	4.21	0.14	4	Y	A	T
1981350	Caboc	4.53	2.55	0.09	3.79	0.10	4	Y	A	T
1982028	Jornada	5.76	4.43	0.09	5.67	0.16	4	Y	B	T
1982043	Molbo	5.48	4.09	0.14	5.33	0.19	4	P	B	R
1982043	Hosta	5.76	4.18	0.13	5.42	0.17	4	P	A	R
1982107	Tenaja	4.49	2.72	0.10	3.95	0.16	4	Y	A	T
1982115	Gibne	5.47	4.11	0.11	5.35	0.18	4	P	A	T
1982126	Kryddost	4.19	2.15	0.12	3.46	0.14	2	Y	A	T
1982127	Bouschet	5.66	4.04	0.12	5.28	0.19	4	Y	B	T
1982167	Kesti	4.01	2.19	0.23	3.43	0.25	3	Y	A	T
1982175	Nebbiolo	5.73	4.26	0.17	5.50	0.25	4	P	A	R

(*continued*)

Table 3
(*Continued*)

			M+B		R+P					
Date	Name	m_b	M_s	std	M_s	std	#	A	W	L
1982210	Monterey	4.68	2.56	0.15	3.80	0.17	4	Y	A	T
1982217	Atrisco	5.82	4.49	0.15	5.73	0.21	4	Y	B	T
1982266	Frisco	4.76	3.08	0.03	4.32	0.15	3	Y	A	T
1982266	Huron Landing	4.88	3.12	0.08	4.35	0.12	3	R	A	T
1982316	Seyval	4.18	2.35	0.22	3.56	0.05	2	Y	A	A
1982344	Manteca	4.72	2.82	0.14	4.06	0.22	4	Y	A	A
1983085	Cabra	5.36	3.90	0.18	5.13	0.26	3	P	A	R
1983104	Turquoise	5.64	4.04	0.09	5.28	0.15	4	Y	B	T
1983112	Armada	4.15	2.37	0.05	3.59	0.06	3	Y	A	T
1983125	Crowdie	4.37	2.35	0.08	3.64	0.05	3	Y	A	A
1983146	Fahada	4.52	3.02	0.16	4.26	0.22	4	Y	A	T
1983160	Danablu	4.73	2.63	0.11	3.90	0.07	2	Y	A	A
1983215	Laban	4.48	2.17	0.07	3.48	0.08	2	Y	A	A
1983223	Sabado	4.17	2.34	0.12	3.63	0.08	3	Y	A	T
1983239	Jarlsberg	3.87	2.07	0.25	3.35	0.21	2	Y	–	–
1983244	Chancellor	5.52	4.02	0.17	5.31	0.16	3	P	A	R
1983264	MidniteZ	4.04	2.53	0.18	3.77	0.17	4	R	A	T
1983265	Techado	4.2	2.25	0.11	3.49	0.14	4	Y	B	T
1983350	Romano	4.97	3.57	0.12	4.79	0.18	3	Y	A	T
1984031	Gorbea	4.51	2.62	0.08	3.85	0.09	4	Y	A	T
1984061	Tortugas	5.82	4.35	0.11	5.56	0.19	3	Y	B	T
1984091	Agrini	4.35	2.79	0.01	3.96	0.11	2	Y	A	A
1984122	Mundo	5.47	4.12	0.02	5.32	0.14	2	Y	B	T
1984152	Caprock	5.61	4.37	0.19	5.58	0.22	3	Y	B	T
1984207	Kappeli	5.62	4.20	0.13	5.41	0.24	3	P	A	R
1984215	Correo	4.57	2.73	0.12	3.97	0.19	4	Y	A	T
1984243	Dolcetto	4.49	2.98	0.11	4.19	0.12	3	Y	A	T
1984257	Breton	4.98	3.44	0.05	4.68	0.13	4	Y	A	T
1984276	Vermejo	4.28	2.39	0.11	3.59	0.04	2	Y	–	–
1984315	Villita	3.9	2.56	0.21	3.80	0.11	4	Y	A	A
1984344	Egmont	5.51	4.10	0.09	5.34	0.18	4	P	A	T
1984350	Tierra	5.64	4.09	0.17	5.33	0.24	4	P	A	R
1985074	Vaughn	4.42	2.88	0.08	4.17	0.11	3	Y	A	T
1985082	Cottage	5.19	3.91	0.00	5.23	0.00	1	Y	A	T
1985096	Misty Rain	4.7	3.18	0.12	4.42	0.21	4	R	A	T
1985122	Towanda	5.63	4.27	0.15	5.51	0.23	4	P	B	T
1985163	Salut	5.62	4.17	0.14	5.41	0.16	4	P	A	R
1985177	Maribo	4.32	2.45	0.10	3.69	0.12	4	Y	A	T
1985206	Serena	5.48	4.24	0.16	5.52	0.13	3	P	A	R
1985270	Ponil	4.49	3.04	0.15	4.27	0.13	4	Y	A	T
1985282	Diamond Beech	4.01	2.12	0.08	3.36	0.12	4	R	A	T
1985289	Roquefort	4.62	2.90	0.15	4.14	0.06	4	Y	A	T
1985339	Kinibito	5.6	4.10	0.13	5.32	0.19	3	Y	B	T
1985362	Goldstone	5.45	4.11	0.14	5.35	0.07	4	P	A	R
1986081	Glencoe	5.41	3.61	0.06	4.83	0.14	3	Y	B	T
1986100	Mighty Oak	4.93	3.26	0.06	4.46	0.22	2	R	A	T
1986112	Jefferson	5.48	4.21	0.04	5.43	0.12	3	P	A	R
1986141	Panamint	3.78	2.14	0.05	3.36	0.08	3	Y	A	A
1986156	Tajo	5.29	3.93	0.00	5.25	0.00	1	Y	A	T
1986176	Darwin	5.58	4.18	0.11	5.39	0.21	3	P	A	T
1986198	Cybar	5.57	4.24	0.06	5.47	0.15	3	P	A	R
1986205	Cornucopia	4.3	2.56	0.14	3.78	0.11	3	Y	A	A
1986247	Galveston	3.71	2.24	0.09	3.51	0.05	2	P	A	R
1986273	Labquark	5.54	4.20	0.13	5.50	0.13	2	P	A	R
1986289	Belmont	5.56	4.25	0.07	5.48	0.15	3	P	A	T
1986318	Gascon	5.58	4.21	0.00	5.53	0.00	1	Y	B	T
1986347	Bodie	5.52	4.30	0.00	5.61	0.00	1	P	A	T
1987042	Tornero	4.24	2.19	0.13	3.42	0.08	3	Y	A	T
1987077	Middle Note	4.22	2.51	0.20	3.72	0.04	2	R	A	T
1987108	Delamar	5.51	4.12	0.08	5.35	0.14	3	P	A	T

(*continued*)

Table 3
(*Continued*)

			M+B		R+P					
Date	Name	m_b	M_s	std	M_s	std	#	A	W	L
1987120	Hardin	5.54	4.22	0.06	5.44	0.17	3	P	A	T
1987169	Brie	4.15	1.96	0.11	3.20	0.20	3	Y	A	T
1987225	Tahoka	5.72	4.35	0.00	5.67	0.00	1	Y	B	T
1987267	Lockney	5.61	4.31	0.12	5.62	0.13	2	P	A	T
1987336	Mission Cyber	3.99	2.21	0.06	3.43	0.16	4	R	A	T
1988046	Kernville	5.48	4.10	0.20	5.31	0.26	3	P	A	T
1988134	Schellbourne	4.77	3.12	0.07	4.33	0.12	3	P	A	A
1988142	Laredo	4.27	2.48	0.18	3.72	0.24	4	Y	–	–
1988154	Comstock	5.58	4.03	0.06	5.23	0.10	2	P	B	T
1988189	Alamo	5.78	4.21	0.19	5.44	0.32	3	P	B	R
1988230	Kearsarge	5.64	4.25	0.24	5.49	0.30	4	P	A	T
1988243	Bullfrog	5.04	3.38	0.04	4.62	0.09	4	Y	A	T
1988287	Dalhart	5.67	4.43	0.13	5.67	0.17	4	Y	B	T
1988345	Misty Echo	4.79	3.37	0.25	4.66	0.23	3	R	A	T
1989041	Texarkana	5.32	3.77	0.02	5.00	0.13	3	Y	–	–
1989055	Kawich-Red	4.41	2.65	0.17	3.89	0.04	3	Y	A	T
1989068	Ingot	4.86	3.14	0.25	4.37	0.38	3	Y	A	T
1989135	Palisade-1	4.55	2.49	0.08	3.72	0.08	3	Y	A	T
1989146	Tulia	3.7	2.08	0.11	3.32	0.02	3	Y	A	T
1989173	Contact	5.43	3.94	0.07	5.17	0.19	3	P	A	T
1989178	Amarillo	5.03	3.30	0.24	4.53	0.24	3	P	B	R
1989257	Disko Elm	4.04	2.28	0.20	3.52	0.18	4	R	A	T
1989304	Hornitos	5.83	4.19	0.13	5.42	0.20	4	P	–	–
1989342	Barnwell	5.56	4.05	0.13	5.29	0.17	4	P	A	T
1990069	Metropolis	5.16	3.47	0.12	4.71	0.18	4	Y	A	T
1990164	Bullion	5.96	4.57	0.15	5.80	0.21	4	P	–	–
1990172	Austin	4.21	2.59	0.14	3.83	0.12	4	Y	A	T
1990206	Mineral Quarry	4.53	2.91	0.20	4.15	0.21	4	R	A	T
1990318	Houston	5.46	3.91	0.15	5.15	0.22	4	P	A	T
1991067	Coso-Bronze	4.51	2.50	0.28	3.71	0.20	3	Y	A	T
1991094	Bexar	5.65	4.22	0.12	5.44	0.22	3	P	–	–
1991257	Hoya	5.69	4.31	0.13	5.52	0.24	3	P	–	–
1991262	Distant Zenith	4.09	2.49	0.17	3.70	0.13	3	R	A	T
1991291	Lubbock	5.16	3.33	0.05	4.55	0.13	3	Y	A	T
1991330	Bristol	4.79	3.13	0.13	4.34	0.17	3	Y	A	T
1992086	Junction	5.81	4.17	0.13	5.38	0.19	3	P	–	–
1992175	Galena-Yellow	4.13	2.30	0.19	3.52	0.16	3	Y	–	–
1992262	Hunters-Trophy	4.18	2.55	0.11	3.76	0.03	3	R	A	T

Date is the year and Julian day for the explosion, Name is the explosion code name, and m_b is the DTV m_b(P*n*) for the event. For each Marshall and Basham (1972) (M + B) and Rezapour and Pearce (1998) (R + P) estimated M_s(7), there is a standard deviation (std) for the given number of stations (#). A, W, and L are the test area (P, Pahute; R, Rainer; Y, Yucca), water table location relative to the explosion (A, above; B, below), and lithology (A, alluvium, T, tuff; R, rhyolite), respectively.

than the Woods and Harkrider (1995) estimates. Woods and Harkrider (1995) showed that their measurements also correlated very well with conventional NTS M_s values from Basham (1969), Marshall and Basham (1972), Basham and Horner (1973), von Seggern (1973), Marshall *et al.* (1979), and Yacoub (1983) with considerable variance in the offsets. We also compared the performance of $\overset{M+B}{M_s}(7)$ and $\overset{R+P}{M_s}(7)$ with Yacoub (1983). The results for the comparison with Yacoub (1983) are also shown in Figure 7 and indicate similar scaling relationships based on the fixed-slope regression analysis. In this case, our $\overset{M+B}{M_s}(7)$ and $\overset{R+P}{M_s}(7)$ values are offset from Yacoub's (1983) estimates by approximately $+0.02$ and $+1.21$ m.u., respectively. Differences in these absolute estimates result from the use of different M_s definitions, especially in the attenuation factors; however, these comparisons do show that our estimates are scaling similarly to other measurements of NTS surface wave magnitudes.

The properties of Rayleigh-wave propagation make it difficult to develop a single expression that gives consistent M_s values at both regional and teleseismic distances. Figure 8 presents the comparison of near-regional M_s estimates [i.e., $\overset{M+B}{M_s}(7)$ and $\overset{R+P}{M_s}(7)$] with far-regional and teleseismic esti-

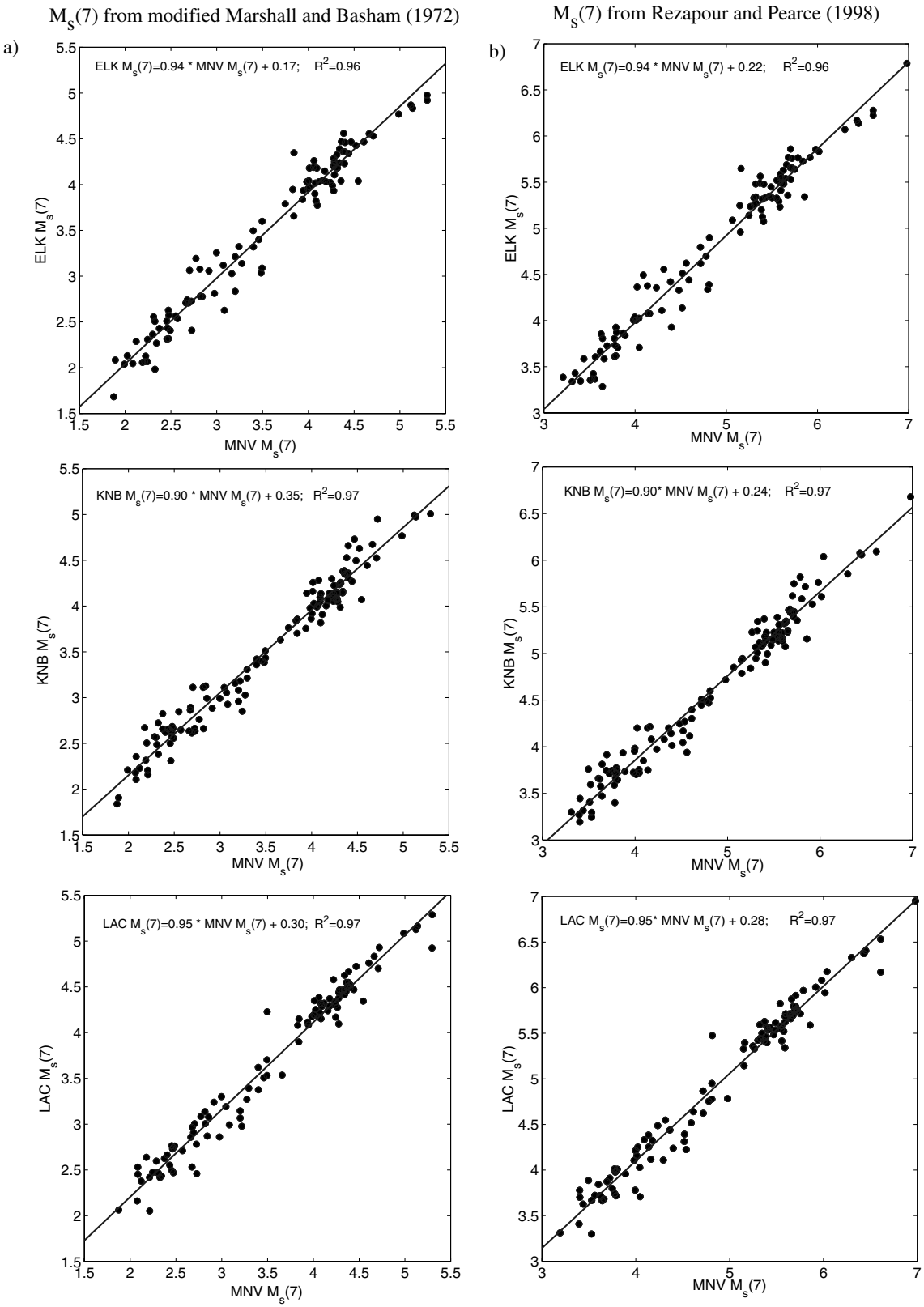

Figure 4. Comparison of (a) $M_s^{M+B}(7)$ and (b) $M_s^{R+P}(7)$ estimates at MNV versus the measurements at ELK (top), KNB (middle), and LAC (bottom). The best least-squares fit to the data is shown as the solid line running through the data points, and the squared correlation coefficients (R^2) are also given.

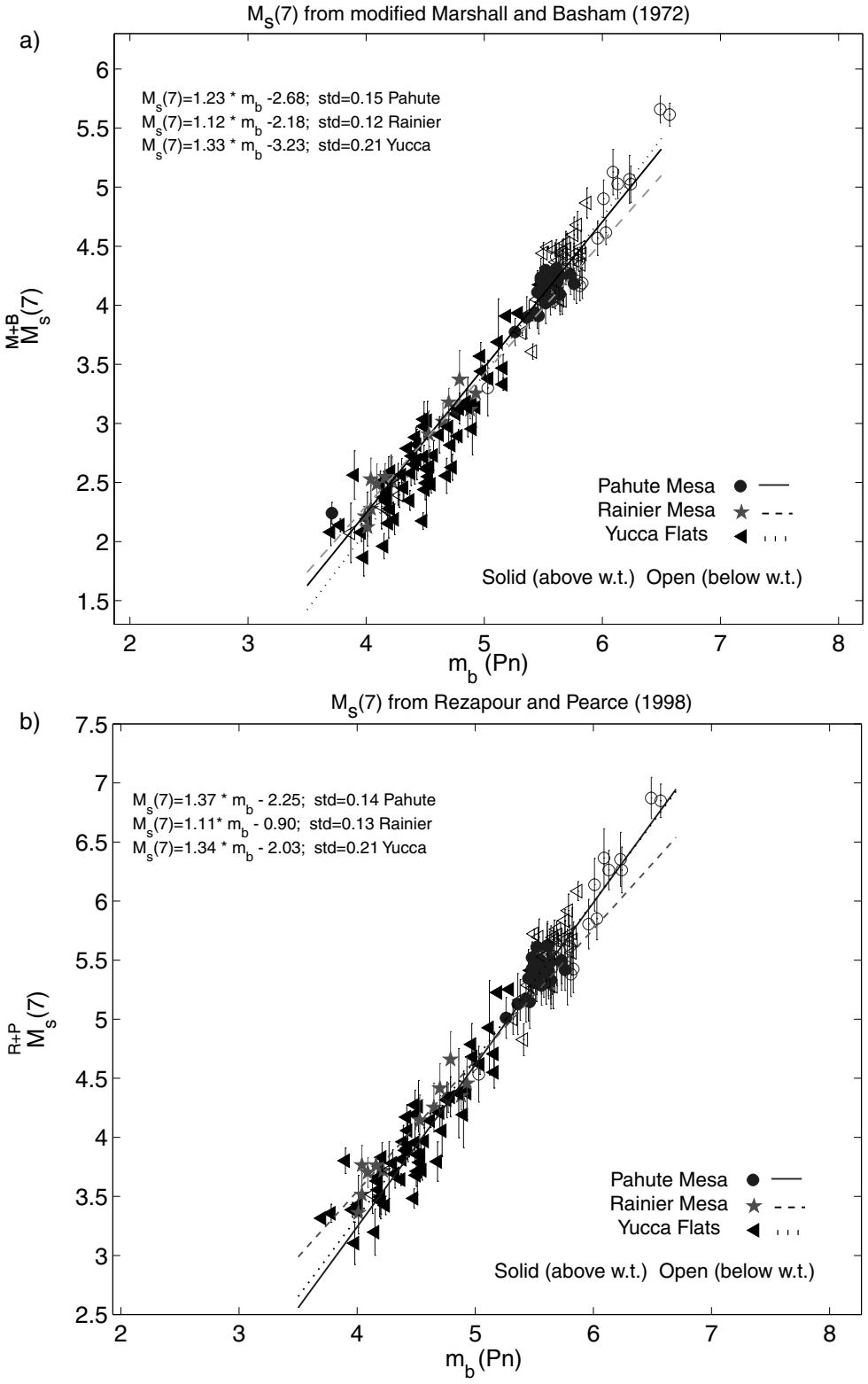

Figure 5. Network-averaged (a) $M_s^{M+B}(7)$ and (b) $M_s^{R+P}(7)$ for 158 NTS events at Pahute Mesa, Rainier Mesa, and Yucca Flats regressed against $m_b(Pn)$. The best-fitting regression lines are plotted as solid (Pahute), dashed (Rainier), and dotted (Yucca) lines. Solid symbols indicate events above the water table (w.t.), with open symbols showing events below the water table. The vertical lines represent one standard deviation for the M_s estimate.

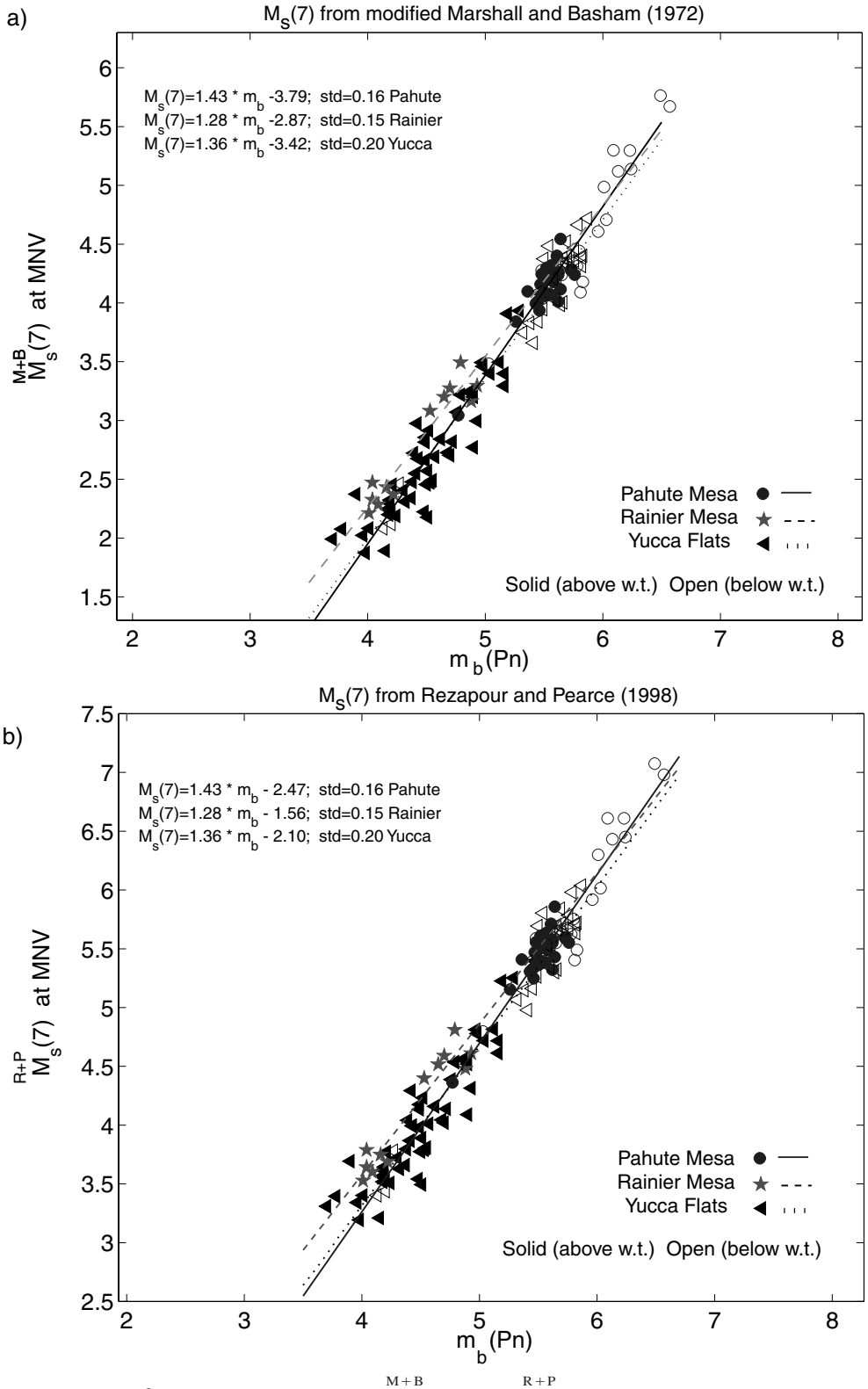

Figure 6. MNV single-station (a) $M_s^{M+B}(7)$ and (b) $M_s^{R+P}(7)$ for NTS events at Pahute Mesa, Rainier Mesa, and Yucca Flats regressed against $m_b(Pn)$.

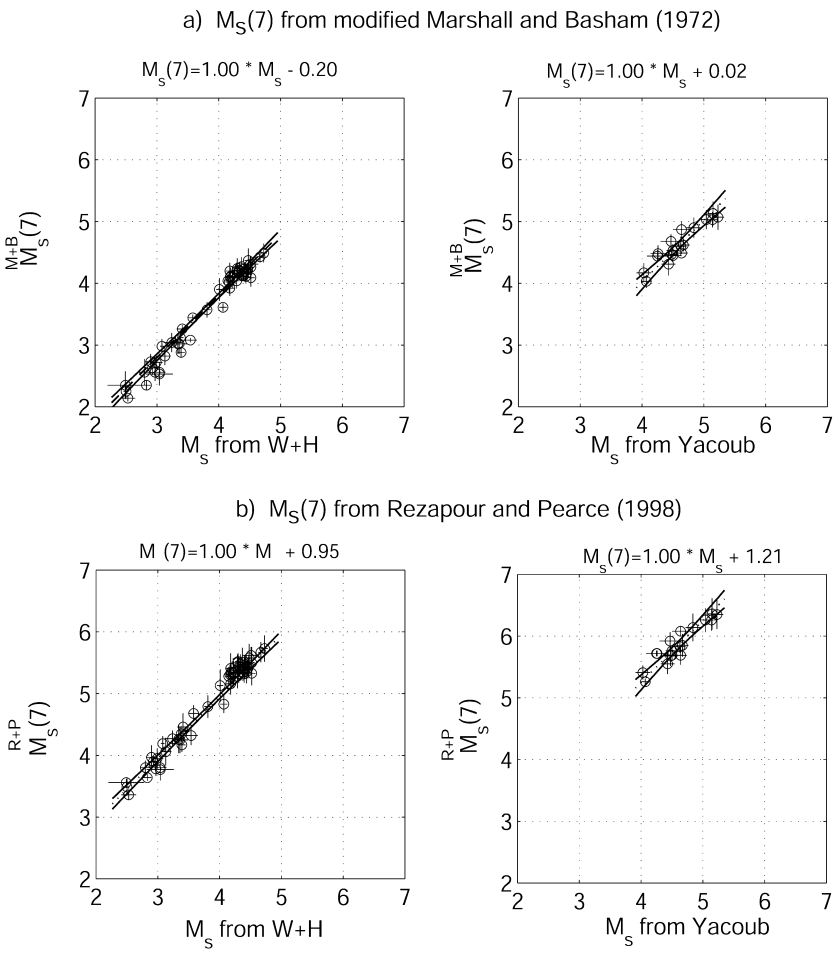

Figure 7. A comparison of our (a) $M_s^{M+B}(7)$ and (b) $M_s^{R+P}(7)$ estimates for NTS with the Woods and Harkrider (1995) indirect estimates (W + H; left) and Yacoub (1983) (right). The best-fitting regression line, with a fixed slope of 1.0, is given by the dotted line running through the data points, and it is surrounded by the pointwise 95% confidence intervals plotted as two solid lines.

mates of M_s using the same formulas (i.e., Marshall and Basham [1972] and Rezapour and Pearce [1998] formulas, respectively). Marshall *et al.* (1979) used the Marshall and Basham (1972) M_s formula for far-regional and teleseismic distance recordings of NTS events for Rayleigh waves with periods greater than 14 sec. We determined that the near-regional $M_s^{M+B}(7)$ estimates have a similar scaling relationship when using a fixed slope (slope = 1.00) regression analysis, but are consistently 0.35 m.u. higher than Marshall *et al.* (1979) for the five events in their dataset for which we had LNN data to analyze. We note that most of our near-regional estimates have better azimuthal coverage than Marshall *et al.* (1979), who mainly used Canadian data and thus may have strong azimuthal biases. This could be a possible source for the bias. Another source could be the attenuation terms; however, we do not have data at a wide enough distance range in this study to verify the appropriateness of Basham (1971) as the correct attenuation model. We observed that the $M_s^{R+P}(7)$ estimates are on average 1.6 m.u. larger than the Marshall *et al.* (1979) teleseismic M_s values.

The Rezapour and Pearce (1998) formula has not been tested significantly at near-regional distances and short periods until this article, and our results suggest there are considerable differences between the short-period, near-regional magnitudes and teleseismic magnitude estimates for NTS events. We regressed our $M_s^{R+P}(7)$ estimates versus far-regional and teleseismic M_s estimates (Fig. 8) determined by Stevens and Murphy (2001) using the Rezapour and Pearce (1998) formula. We note consistent scaling between the two estimates; however, there is an offset of +1.46 m.u. We note much better agreement between the Stevens and Murphy (2001) teleseismic M_s values and the 7-sec modified Marshall and Basham (1972) estimates. Thus, we believe path corrections will be required for correct application of the Rezapour and Pearce (1992) formula at near-regional distances and periods less than 10 sec.

Earthquakes

We measured the amplitude for 7-sec-period Rayleigh waves for 40 earthquakes (Fig. 1) within 2° of the NTS as recorded at MNV (or the collocated NV31), ELK, KNB, and LAC and estimated a $M_s^{M+B}(7)$ and $M_s^{R+P}(7)$ for each event. The results are compiled in Table 4 and are presented in Figures 9 and 10, in addition to the explosion analyses. In Figure 9, we present a comparison of the $M_s^{M+B}(7)$ and $M_s^{R+P}(7)$ estimates for both earthquakes and explosions. We find that to obtain

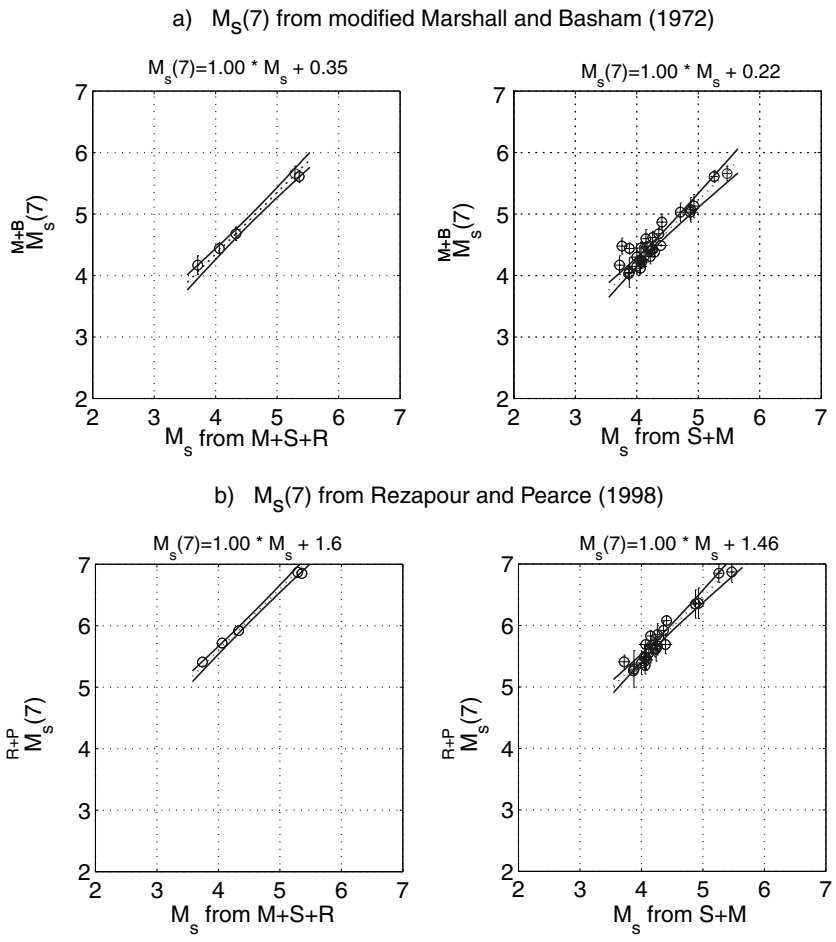

Figure 8. A comparison of our (a) $\overset{M+B}{M}_s(7)$ and (b) $\overset{R+P}{M}_s(7)$ estimates for NTS with the Marshall *et al.* (1979) estimates (M + S + R; left) and Stevens and Murphy (2001) estimates (S + M; right).

an $\overset{M+B}{M}_s(7)$ estimate from an $\overset{R+P}{M}_s(7)$ magnitude, we must subtract 1.23 m.u. for explosions and 1.08 m.u for earthquakes; however, the scatter in the earthquake data is 0.2 m.u larger than for the explosion estimates. In Figure 10, we regressed the $\overset{M+B}{M}_s(7)$ and $\overset{R+P}{M}_s(7)$ versus DTV m_b for both populations. The best-fitting regression lines are plotted and labeled in the figure together with 95% confidence intervals. Although the slopes for each line are different, we do not have enough earthquakes with $m_b > 4.5$ to fully constrain this section of the regression analyses. We also note that the standard deviation for the earthquake data for both plots is a factor of 2 larger than that of the explosions, which could possibly be related to depth effects on 7-sec-period, Rayleigh-wave generation. We compared our earthquake regression results (slope = 1.1, *y* intercept = 1.4, standard deviation [std] = 0.31) with the original Marshall and Basham (1972) results for North American earthquakes recorded at far-regional and teleseismic distances at periods greater than 14 sec (slope = 1.2, *y* intercept = 1.4, std = 0.23). We note similar slopes and *y* intercepts; however, the differences in the standard deviation are caused by near-source and receiver complexities that affect 7-sec Rayleigh waves more drastically than surface waves with periods greater than 14 sec. However, this discrepancy is countered by the ability of our method to estimate M_s for earthquakes with m_b's as small as 3 and explosions with m_b's as small as 3.7 (as compared to 3.8 and 4.5, respectively, for Marshall and Basham [1972]).

Discriminant Analysis

The final objective of this article is to examine the performance of the modified Marshall and Basham (1972) and Rezapour and Pearce (1998) $M_s(7)$-m_b discriminants for earthquakes and explosions. The populations plotted in Figure 10 suggest that M_s and m_b will be fitted well by linear regressions, with approximately equal slopes assumed for the earthquake and explosion populations. Although we did observe slightly different slopes in the regression analyses for the two populations, we believe that this is due to inadequate sampling of earthquakes at m_b magnitudes greater than 4.5. Our dataset does not present any evidence that the two populations are converging at smaller magnitudes, although other M_s-m_b studies (Stevens and McLaughlin, 2001) suggest that convergence does occur. Furthermore, it seems sensible to regard the M_s values as dependent variables, observed conditionally on fixed values for m_b, which are more accurately determined in the WUS when the DTV m_b (Denny *et al.*, 1987, 1989) formula is applied. This yields the following regression model:

Table 4
Earthquake Information

Date (yyyymmdd)	Origin Time (hhmmss)	Latitude	Longitude	Depth	m_b	$\overset{M+B}{M_s}$ (7)	std	$\overset{R+P}{M_s}$ (7)	std	No. Stations
19790812	113119	37.26	115.08	5	3.18	2.33	0.24	3.47	0.47	3
19791225	141710	37.27	117.06	5	3.67	2.95	0.13	4.07	0.19	4
19800115	202822	36.18	117.60	8	3.63	2.64	0.20	3.74	0.17	4
19800225	234332	36.20	117.58	5	3.86	2.73	0.18	3.83	0.22	4
19800527	145057	37.48	118.81	13	5.79	5.40	0.14	6.47	0.27	4
19811201	161850	38.62	118.19	11	4.02	3.41	0.10	4.25	0.35	3
19811219	205652	38.63	118.21	17	4.12	3.20	0.37	4.16	0.29	4
19820124	154407	37.45	117.83	5	4.09	2.82	0.08	3.90	0.31	4
19820316	84700	36.60	117.03	6	3.48	2.80	0.18	3.92	0.20	4
19820512	192924	37.27	115.08	10	3.49	2.46	0.30	3.65	0.44	4
19820706	21043	37.69	115.05	3	4.3	2.97	0.22	4.26	0.23	3
19820924	74024	37.85	118.12	5	4.99	4.09	0.14	5.14	0.34	4
19830604	113740	37.39	115.21	6	3.44	2.36	0.18	3.54	0.27	4
19840802	110134	37.30	114.94	5	3.49	2.14	0.28	3.33	0.35	4
19841123	180825	37.48	118.66	5	5.54	5.15	0.40	6.14	0.42	3
19851210	61025	37.30	115.01	5	3.7	2.85	0.07	3.99	0.19	3
19920629	103102	36.69	116.24	5	4.66	3.71	0.13	4.73	0.29	2
19920629	155239	36.71	116.29	8	3.89	2.36	0.12	3.38	0.54	2
19920629	170116	36.74	116.29	8	3.81	2.49	0.16	3.51	0.26	2
19920630	160624	36.72	116.26	5	3.5	2.24	0.05	3.26	0.37	2
19920705	65412	36.69	116.28	5	4.38	2.92	0.19	3.94	0.23	2
19920705	84838	36.67	116.19	11	3.05	1.99	0.26	3.02	0.15	2
19930517	232049	37.17	117.78	6	5.84	5.67	0.34	6.70	0.45	3
19930518	10306	37.15	117.76	2	4.9	3.81	0.23	4.91	0.22	4
19930518	234853	37.06	117.78	3	4.93	3.94	0.14	5.04	0.32	4
19930519	141322	37.14	117.77	0	5.21	3.94	0.15	5.03	0.20	4
19930520	201414	36.10	117.70	0	4.32	3.52	0.14	4.80	0.19	2
19990125	185207	36.82	115.96	5	4.17	3.19	0	4.51	0	1
19990125	195154	36.81	115.96	5	2.98	2.40	0	3.72	0	1
19990127	104423	36.82	115.99	5	4.48	3.33	0	4.64	0	1
20000228	230842	36.07	117.60	0	3.87	3.08	0	4.40	0	1
20000229	220805	36.08	117.60	0	3.7	2.83	0	4.15	0	1
20000302	150034	36.08	117.60	0	3.68	2.63	0	3.95	0	1
20010517	215357	35.80	118.05	9	3.6	2.73	0	4.04	0	1
20010517	225645	35.80	118.05	8	3.64	2.88	0	4.20	0	1
20010717	120726	36.01	117.86	7	4.94	4.19	0	5.51	0	1
20010717	122518	36.04	117.87	5	3.74	2.97	0	4.29	0	1
20010717	125959	36.02	117.88	0	4.22	3.84	0	5.16	0	1
20020324	100407	37.00	115.70	10	3.77	2.55	0	3.88	0	1
20020614	124044	36.72	116.30	5	3.81	3.50	0.22	4.81	0.24	2

$$M_s = \alpha_i + \beta m_b + e, \tag{4}$$

$i = 1,2$, where the intercepts α_1 and α_2 correspond to the earthquake and explosion populations, respectively. Under this approach, the errors (e) are assumed to be independent and identically distributed normal variables.

For determining the optimal discriminant functions, the parallel regression assumption with independent normal errors seems more sensible than the usual assumption of bivariate normality used to get the classification function. Hence, we proceed to use the linear function following from the conditional regression approach to discrimination. This leads to a discriminant function of the form

$$d = M_s - \frac{1}{2}(\alpha_1 + \alpha_2) - \beta m_b. \tag{5}$$

With equal prior probabilities, we classify an event of unknown origin as an earthquake if $d > 0$ and as an explosion otherwise. Estimating the parameters α_1, α_2, and β for the two M_s populations led to the values given in Table 5.

The classification criterion in the equal slope case is then applied with the values estimated from the data. We note first the result of applying the discriminant function, d, directly, as shown in Figure 11. Note the four misclassified earthquakes in the $\overset{M+B}{M_s}$ (7)-m_b plot and the six misclassified earthquakes in the $\overset{R+P}{M_s}$ (7)-m_b case. To estimate the performance of the discriminant function (equation 5), we used a jackknifing technique where the observation to be classified is held out during the estimation of the slope and intercept procedure and then the discriminant function is applied to the observation to be classified using the estimated param-

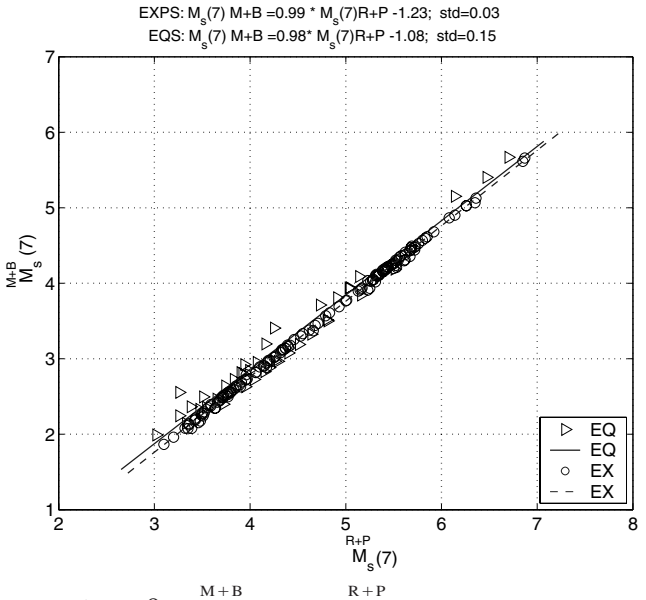

Figure 9. $M_s^{M+B}(7)$ versus $M_s^{R+P}(7)$ estimates for all earthquakes (EQs) and explosions (EXs) considered in this study.

eters. The results are shown in Table 6, and we note that the modified Marshall and Basham $M_s^{M+B}(7)$ values perform better. For the $M_s^{M+B}(7)$ case, we misclassified four earthquakes as explosions (10%) while only classifying two explosions (1.2%) as earthquakes. The misclassification rates are slightly higher for the $M_s^{R+P}(7)$ estimates, as we identified six earthquakes (16%) as explosions and three explosions (2%) as earthquakes. A reviewer has suggested that the slopes may be unequal, and indeed, the hypothesis of unequal slopes can not be statistically rejected for this particular dataset. Following through on the discriminant analysis under the unequal slope assumption leads to results that are slightly worse than those shown in Table 5. We note that there were now five more incorrect decisions for explosions in the $M_s^{M+B}(7)$ case and eight more in the $M_s^{R+P}(7)$ case when the unequal slope case was considered. The inferior performance is taken as providing some evidence that generalizing to the unequal slope case may not be needed.

It is also useful to look at theoretical operating characteristic curves for the two M_s measures. Figure 12 shows the explosion detection probabilities expected for the two measures as a function of the explosion false-alarm probabilities, assuming that the normal theory holds for the discriminant. Note that the $M_s^{M+B}(7)$ curve is better for both a false-alarm probability of 0.01 (0.3 versus 0.7 signal detection probability) and for a false-alarm probability of 0.05 (0.8 versus 0.95 signal detection probability). It is interesting in this case that the signal detection and false-alarm probabilities change primarily as a function of the intercept difference $\delta = \alpha_1 - \alpha_2$, which is substantially larger (1.46 versus 0.79) for the

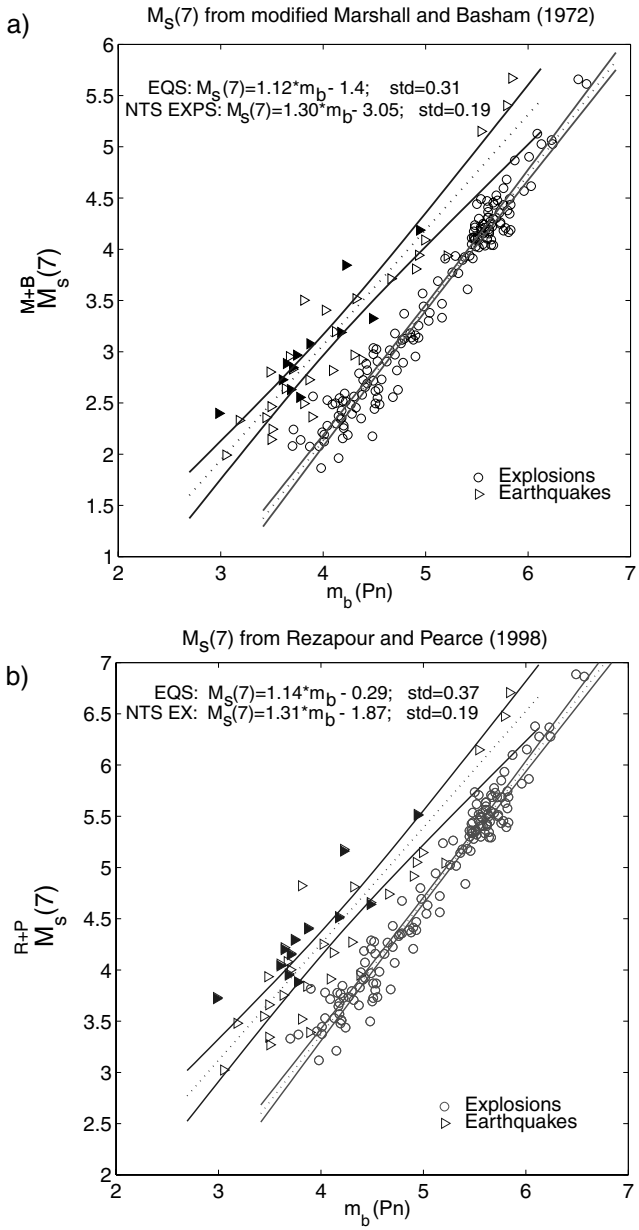

Figure 10. (a) $M_s^{M+B}(7)$-m_b and (b) $M_s^{R+P}(7)$-m_b results for the earthquakes and explosions shown in Figure 1. For each population, the best-fitting regression line is the dotted line running through the data points, surrounded by the pointwise 95% confidence intervals plotted as two solid lines. The earthquakes plotted as solid symbols represent single-station (MNV/NV31) estimates of both $M_s(7)$ and m_b.

Table 5
Intercepts and Slopes for the $M_s^{M+B}(7)$ $M_s^{R+P}(7)$ Estimates

Data	α_1	α_2	β	σ_1	σ_2
$M_s^{M+B}(7)$	−1.99(0.10)	−2.87(0.12)	1.26(0.02)	0.334	0.192
$M_s^{R+P}(7)$	−0.78(0.11)	−1.57(0.13)	1.25(0.03)	0.391	0.195

Standard errors are in parentheses.

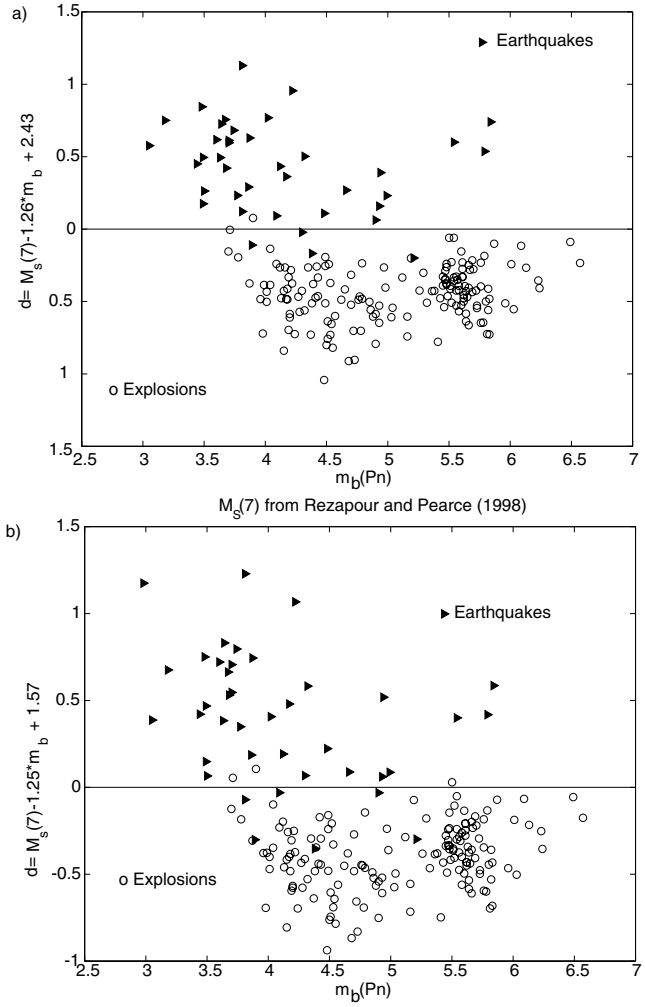

Figure 11. Discriminant functions for (a) $M_s^{M+B}(7)$-m_b and (b) $M_s^{R+P}(7)$-m_b for earthquakes and explosions considered in this study. The parameter a from equation (4) represents the slope (1.26 and 1.25) of the m_b versus M_s populations, and the decision line is determined from the means for both populations. Based upon our evaluation of the $M_s^{M+B}(7)$-m_b relationship for this region, we calculated the probability of misclassifying an earthquake as an explosion as 10% and the probability of classifying an explosion as an earthquake as 1.2%. The results are slightly worse for $M_s^{R+P}(7)$-m_b, where 15% of the earthquakes are misclassified as explosions and 2% of the explosions are labeled as earthquakes.

Table 6

Jackknifed Corrected Decisions and Errors for Earthquakes (Q) and Explosions (X)

	Correct		Incorrect	
Model	Q	X	Q	X
$M_s^{M+B}(7)$	36	156	4	2
$M_s^{R+P}(7)$	34	155	6	3

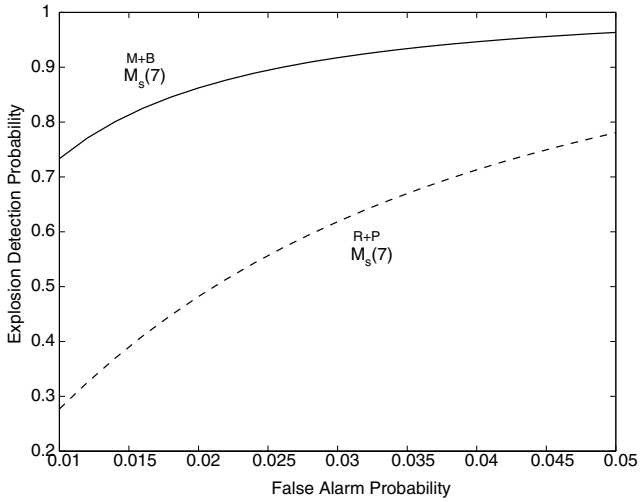

Figure 12. Explosion detection as a function of false alarm probability for the linear discriminants using the modified Marshall and Basham (1972) and Rezapour and Pearce (1998) $M_s(7)$ estimates.

$M_s^{M+B}(7)$ and $M_s^{R+P}(7)$ populations, respectively. The suspected cause of the differences in the M_s-m_b discriminant performance arises from the use of empirical path corrections for the Marshall and Basham (1972) estimates as compared to none for Rezapour and Pearce (1998). This study suggests that path correction makes a substantial difference in the discrimination performance for this technique.

Conclusions

The $M_s^{M+B}(7)$-m_b and $M_s^{R+P}(7)$-m_b discriminants defined in this article can now be used as tools to help screen explosions from earthquakes in the vicinity of the NTS. The false classification rates for the method are small, and the method can be used in conjunction with other regional NTS discriminants, such as the phase and spectral ratios (Walter *et al.*, 1995) and body wave and moment magnitude ratios (m_b-M_W) (Patton, 2001).

Transportability of the $M_s^{M+B}(7)$-m_b discriminant to regions other than NTS will be complicated due to bias in small-magnitude m_b measurements, deeper events, variable path lengths, and more complex propagation paths. Thus, our attempts to transport the discriminant will require both accurate m_b estimates for regional events in different regions of the world using techniques such as coda m_b (Mayeda, 1993) and $m_b(Lg)$ (Patton, 2001) as well as high-quality dispersion curves in the period range of 5–20 sec in order to estimate path corrections for $M_s^{M+B}(7)$. For the latter, the research efforts of Levshin *et al.* (2002), who have been developing group velocity maps for Rayleigh waves recorded in Asia with periods of 7 sec and greater, will be extremely beneficial to our attempts at transporting this technique.

Acknowledgments

We are indebted to Howard Patton for his assistance in database acquisition and his comments concerning various aspects of the research. We also wish to thank Bill Walter for help in acquiring the MNV dataset. We express our gratitude to Marv Denny, Jeff Stevens, Steve Taylor, Nancy Cunningham, Delaine Reiter, Shelly Johnson, and James Lewkowicz for insightful discussions about the manuscript and research. Constructive comments from an anonymous reviewer were greatly appreciated. We thank the developers of the Generic Mapping Tools software (Wessel and Smith, 1998), Computer Programs in Seismology (Herrmann, 2002), and Matlab, which were all used to generate and present the results of our research. This research was sponsored by the Defense Threat Reduction Agency under Contract Number DTRA01-01-C-0080.

References

Basham, P. W. (1971). A new magnitude formula for short-period continental Rayleigh waves, *Geophys. J. R. Astr. Soc.* **23,** 255–260.

Basham, P. W., and R. B. Horner (1973). Seismic magnitudes of underground nuclear explosions, *Bull. Seism. Soc. Am.* **63,** 105–131.

Bath, M. (1952). Earthquake magnitude determination from the vertical component of surface waves, *Trans. Am. Geophys. Un.* **33,** 81.

Chael, E. P. (1997). An automated Rayleigh-wave detection algorithm, *Bull. Seism. Soc. Am.* **87,** 157–163.

Day, S. M., and K. L. McLaughlin (1991). Seismic source representation for spall, *Bull. Seism. Soc. Am.* **81,** 191–201.

Denny, M. D., S. R. Taylor, and E. S. Vergino (1987). Investigation of m_b and M_s formulas for the western United States and their impact on the M_s/m_b discriminant, *Bull. Seism. Soc. Am.* **77,** 987–995.

Denny, M. D., S. R. Taylor, and E. S. Vergino (1989). Erratum: Investigation of m_b and M_s formulas for the western United States and their impact on the M_s/m_b discriminant, *Bull. Seism. Soc. Am.* **79,** 230.

Dziewonski, A. M., J. Bloch, and M. Landisman (1969). A new technique for the analysis of transient seismic signals, *Bull. Seism. Soc. Am.* **59,** 427–444.

Evernden, J. F. (1971). Variation of Rayleigh-wave amplitude with distance, *Bull. Seism. Soc. Am.* **61,** 231.

Ewing, W. M., F. Press, and W. S. Jardetzky (1957). *Elastic Waves in Layered Media*, McGraw-Hill, New York.

Gutenberg, B. (1945). Amplitudes of surface waves and the magnitudes of shallow earthquakes, *Bull. Seism. Soc. Am.* **35,** 3.

Herrin, E. T., and T. Goforth (1977). Phase-match filtering: application to the study of Rayleigh waves, *Bull. Seism. Soc. Am.* **67,** 1259–1275.

Herrmann, R. B. (2002). *Computer Programs in Seismology*, version 3.15, St. Louis University.

Keller, G. R., R. B. Smith, L. W. Braile, R. Heaney, and D. H. Shurbet (1976). Upper crustal structure of the eastern Basin and Range, northern Colorado plateau, and middle Rocky Mountains from Rayleigh-wave dispersion, *Bull. Seism. Soc. Am.* **67,** 869–876.

Levshin, A., J. Stevens, M. Ritzwoller, and D. Adams (2002). Short-period (7-s to 15-s) group velocity measurements and maps in central Asia, *Proc. of the 24th Seismic Research Review on Nuclear Explosion Monitoring: Innovation and Integration*, Ponte Vedra Beach, Florida, 17–19 September 2002.

Marshall, P. D., and P. W. Basham (1972). Discrimination between earthquakes and underground explosions employing an improved M_s scale, *Geophys. J. R. Astr. Soc.* **29,** 431–458.

Marshall, P. D., D. L. Springer, and H. C. Rodean (1979). Magnitude corrections for attenuation in the upper mantle, *Geophys. J. R. Astr. Soc.* **57,** 609–638.

Mayeda, K. M. (1993). m_b(*Lg*Coda): a stable single station estimator of magnitude, *Bull. Seism. Soc. Am.* **83,** 851–861.

Patton, H. (1991). Seismic moment estimation and the scaling of the explosion source, in *Explosion Source Phenomenology*, S. R. Taylor, H. J. Patton, and P. G. Richards (Editors), American Geophysical Monograph 65, 171–183.

Patton, H. (2001). Regional magnitude scaling, transportability, and M_s-m_b discrimination at small magnitudes, in *Monitoring the Comprehensive Nuclear Test Ban Treaty: Source Processes and Explosion Yield Determination*, G. Ekstrom, M. Denny, and J. R. Murphy (Editors), *Pure Appl. Geophys.* **158,** 1951–2015.

Rezapour, M., and R. G. Pearce (1998). Bias in surface-wave magnitude M_s due to inadequate distance correction, *Bull. Seism. Soc. Am.* **88,** 43–61.

Selby, N. (2001). Association of Rayleigh waves using backazimuth measurements: application to test ban verification, *Bull. Seism. Soc. Am.* **91,** 580–593.

Stevens, J. L., and K. L. McLaughlin (2001). Optimization of surface wave identification and measurement, in *Monitoring the Comprehensive Nuclear Test Ban Treaty: Surface Waves*, A. Levshin, and M. H. Ritzwoller (Editors), *Pure Appl. Geophys.* **158,** 1547–1582.

Stevens, J. L., and J. R. Murphy (2001). Yield estimation from surface-wave amplitudes, in *Monitoring the Comprehensive Nuclear Test Ban Treaty: Surface Waves—Source Processes and Explosion Yield Determination*, G. Ekstrom, M. Denny, and J. R. Murphy (Editors), *Pure Appl. Geophys.* **158,** 2227–2251.

Stevens, J. L., D. A. Adams, and E. Baker (2001). Surface wave detection and measurement using a one-degree global dispersion grid, SAIC Final Report, SAIC-01/1085, Alexandria, Virginia.

Taylor, S. R., and G. E. Randall (1989). The effects of spall on regional seismograms, *Geophys. Res. Lett.* **16,** 211–221.

Tibuleac, I. M., J. L. Bonner, E. T. Herrin, and D. G. Harkrider (2002). Calibration of the M_s-m_b discriminant at NVAR, *Proc. of the 24th Seismic Research Review on Nuclear Explosion Monitoring: Innovation and Integration*, Ponte Vedra Beach, Florida, 17–19 September 2002.

Vanek, J., A. Zatopek, V. Karnik, Y. V. Riznichenko, E. F. Saverensky, S. L. Solov'ev, and N. V. Shebalin (1962). Standardization of magnitude scales, *Bull. (Izvest.) Acad. Sci. U.S.S.R. Geophys. Ser.* **2,** 108.

Vergino, E. S., and R. W. Mensing (1989). Yield estimation using regional m_b(Pn), Lawrence Livermore National Laboratory Report UCID-101600, Lawrence Livermore National Laboratory, Livermore, California.

von Seggern, D. (1973). Joint magnitude determination and analysis of variance for explosion magnitude estimates, *Bull. Seism. Soc. Am.* **63,** 827–845.

von Seggern, D. (1977). Amplitude distance relation for 20-second Rayleigh waves, *Bull. Seism. Soc. Am.* **67,** 405–411.

Walter, W. R., K. M. Mayeda, and H. J. Patton (1995). Phase and spectral ratio discrimination between NTS earthquakes and explosions. I. Empirical observations, *Bull. Seism. Soc. Am.* **85,** 1050–1067.

Wessel, P., and W. H. F. Smith (1998). New, improved version of the Generic Mapping Tools released, *EOS* **79,** 579.

Woods, B., and D. G. Harkrider (1995). Determining surface-wave magnitudes from regional Nevada Test Site data, *Geophys. J. Int.* **120,** 474–498.

Yacoub, N. K. (1983). Instantaneous amplitudes: a new method to measure seismic magnitude, *Bull. Seism. Soc. Am.* **73,** 1345–1355.

Yang, X., R. North, and C. Romney (2000). CMR Nuclear Explosion Database, Center for Monitoring Research, Technical Report CMR-0016, Alexandria, Virginia, 129 pp.

Zhao, L. S., and D. G. Harkrider (1992). Wavefields from an off-center explosion in an imbedded solid sphere, *Bull. Seism. Soc. Am.* **82,** 1927–1955.

Weston Geophysical Corporation
4000 S. Medford, Suite 10W
Lufkin, Texas 75901
bonner@westongeophysical.com
(J.L.B.)

Weston Geophysical Corporation
57 Bedford Street, Suite 102
Lexington, Massachusetts 02420
hark@mvl7-2-1.ourconcord.net
sara@westongeophysical.com
ileana@westongeophysical.com
(D.G.H., S.A.R., I.M.T.)

Southern Methodist University
P.O. Box 0395
Dallas, Texas 75275
herrin@passion.isem.smu.edu
(E.T.H.)

Department of Statistics
University of California
360 Kerr Hall
One Shields Ave.
Davis, California 95616
rhshumway@ucdavis.edu
(R.H.S.)

Manuscript received 6 December 2002.